Different Mechanisms For Dynamical Arrest In Largely Asymmetric Binary Mixtures

Different mechanisms for dynamical arrest in largely asymmetric binary mixtures

J. Hendricks,[1] R. Capellmann,[1] A. B. Schofield,[2] S. U. Egelhaaf,[1] and M. Laurati[1,*]

[1]*Condensed Matter Physics Laboratory, Heinrich-Heine University, Universitätsstr. 1, 40225 Düsseldorf, Germany*

[2]*SUPA, School of Physics & Astronomy, University of Edinburgh, Peter Guthrie Tait Road, Edinburgh EH9 3FD, United Kingdom*

(Received 6 November 2014; revised manuscript received 30 January 2015; published 16 March 2015)

Using confocal microscopy we investigate binary colloidal mixtures with large size asymmetry, in particular the formation of dynamically arrested states of the large spheres. The volume fraction of the system is kept constant, and as the concentration of small spheres is increased we observe a series of transitions of the large spheres to different arrested states: an attractive glass, a gel, and an asymmetric glass. These states are distinguished by the degree of dynamical arrest and the amount of structural and dynamical heterogeneity. The transitions between two different arrested states occur through melting and the formation of a fluid state. While a space-spanning network of bonded particles is found in both arrested and fluid states, only arrested states are characterized by the presence of a space-spanning network of dynamically arrested particles.

DOI: 10.1103/PhysRevE.91.032308 PACS number(s): 64.70.pv, 61.43.−j, 63.50.Lm, 83.80.Kn

I. INTRODUCTION

The glass transition in model one-component hard-sphere colloidal dispersions has been the subject of many studies [1–7]. The formation of a glass state for volume fractions $\phi > 0.58$ is due to the dynamical arrest of particles in cages formed by their neighbors. Only activated processes can release the constraints that limit the motion of the particles to the in-cage space and then lead to diffusion [6].

Addition of a second component with a different size affects the glass transition [8–23]. For moderate size disparities, $\delta = R_s/R_L \gtrsim 0.35$, mixing particles with different radii R_s and R_L, respectively, results in a shift of the glass transition to larger total volume fractions ϕ, similar to the effect of polydispersity [8–10]. On the other hand if the size disparity is larger, $\delta \lesssim 0.35$, depending on the mixing ratio $x_s = \phi_s/\phi$, with ϕ_s the volume fraction of small spheres, different glass states have been predicted by mode-coupling theory (MCT) and the self-consistent generalized Langevin equation theory (SCGLE) [10–12,16].

The different glass states are distinguished by the arrest mechanism of the large spheres and the mobility of the small spheres. At small x_s, a double glass is expected, in which both species are arrested through caging of spheres of the same species, and in addition the large particles might be bonded. At intermediate x_s a single glass occurs, in which only the large particles are arrested while the small particles are still mobile; for $\delta \gtrsim 0.2$ the large particles are expected to always form an attractive glass, while for smaller δ a repulsive glass is also predicted. At large x_s, an asymmetric or *torroncino* glass forms, in which the large particles are localized in a glass of small spheres. Furthermore, it has been proposed that equilibrium gel states of the large spheres form at intermediate x_s due to the oscillatory form of the effective potential [16].

The existence of some of these states has been verified in experiments and simulations. A transition from a double glass to an asymmetric glass was recently observed in experiments for $\delta = 0.2$ [18,19], showing similarities with simulations on soft spheres [14,15] and asymmetric mixtures of star polymers [24,25]. This change in caging mechanism is responsible for glass softening, facilitated yielding and acceleration of the dynamics of the large particles under shear at intermediate x_s [18,19]. Dynamically arrested states of the large spheres in which the smallest component remains mobile have been observed experimentally at $\delta \approx 0.1$ [13] and in simulations [14,15].

Despite these findings, a systematic investigation of dynamically arrested states in largely asymmetric hard-sphere mixtures with $\delta \lesssim 0.2$ is still missing. In particular an experimental characterization of the theoretically predicted different arrested states of the large spheres as a function of the composition x_s and the total volume fraction ϕ and a discussion of the role of depletion interactions and bonding at these large size disparities are still missing.

Here we investigate, using confocal microscopy and particle tracking, the occurrence of dynamically arrested states in binary mixtures of hard-sphere colloids with size ratio $\delta \approx 0.09$ and fixed total volume fraction $\phi \approx 0.60$ [26]. We analyze the average dynamics of the large particles in the mixtures through the mean squared displacements to reveal dynamically arrested states, and we determine the presence and spatial distribution of dynamical heterogeneities. We complement this dynamical information with information on the arrangement of the large particles, namely, their pair distribution function, the distribution of the number of bonds, and the organization of bonded particles into clusters and eventually into a network, as well as the degree of structural heterogeneity. Combining the dynamical and structural information we reveal the existence of repulsive and attractive glasses at small x_s, a gel state at intermediate x_s, and an asymmetric glass of clusters at large x_s. The transition between the glass states involves the melting of the glasses and the occurrence of fluid states.

II. MATERIALS AND METHODS

A. Samples

The samples are mixtures of polymethylmethacrylate (PMMA) colloids with radii of the large spheres $R_L = 720 \pm 30$ nm (labeled with NBD), as determined by static light scattering, and radii of the small spheres $R_s = 65 \pm 10$ nm

*marco.laurati@uni-duesseldorf.de

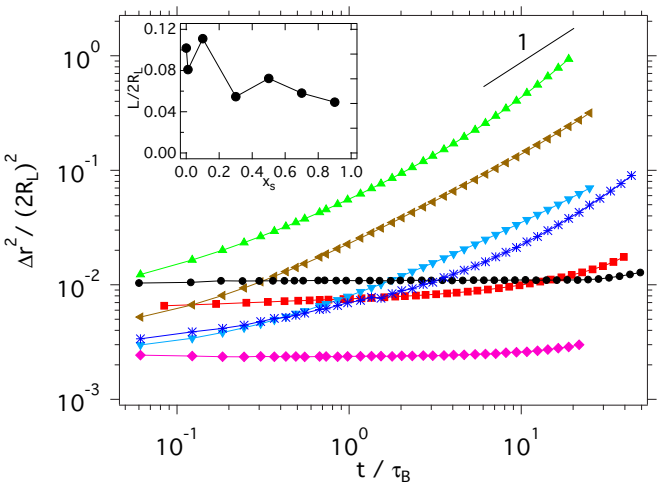

FIG. 1. (Color online) Mean squared displacements of the large spheres, $\Delta r^2/(2R_L)^2$, for samples with total volume fraction $\phi \approx 0.60$, size ratio $\delta = 0.09$, and different compositions $x_s = 0.0$ (●), 0.01 (■), 0.1 (▲), 0.3 (▼), 0.5 (◀), 0.7 (∗), 0.9 (♦). Inset: Localization length $L/(2R_L)$ as a function of x_s.

(labeled with $DiIC_{18}$), as determined by dynamic light scattering, corresponding to a size ratio $\delta = R_L/R_s = 0.09$. The polydispersity of the large spheres, $\sigma_L \approx 13\%$, was also estimated by static light scattering. For the small spheres, the absence of crystallization in the quiescent and sheared state suggests $\sigma_s > 12\%$ [27]. Particles are dispersed in a mixture of cis-decalin and cyclohexylbromide (CHB), which closely matches their density and refractive index. In this solvent mixture the particles acquire a charge, which is screened by adding 4 mM tetrabutylammoniumchloride (TBAC) [28]. Under these conditions the particle interactions are hard-spherelike [26].

A sediment of the large particles with $\phi = 0.66$, as estimated from comparison with numerical simulations [29], is diluted to yield a one-component dispersion of large spheres with $\phi \approx 0.60$, where, following a recent study [30], the uncertainty $\Delta\phi$ can be as large or above 3%. Nevertheless the arrested dynamics of this dispersion (Fig. 1) indicate $\phi > 0.58$. The sample of large spheres with $\phi \approx 0.60$ is used as a reference. The volume fraction of a glass sample containing only small particles is adjusted in order to obtain comparable linear viscoelastic moduli after normalization of the viscoelastic moduli with the energy density $3k_BT/4\pi R^3$, where k_BT is the thermal energy, and the frequency by the inverse free-diffusion Brownian time $\tau_0^{-1} = D_0/R^2 = k_BT/6\pi\eta R^3$, where $\eta = 2.2$ mPa s is the solvent viscosity. For our system the ϕ-dependent short-time Brownian time of the large spheres was estimated as $\tau_B = R_L^2/D_L(\phi) \approx 56$ s, with $D_L(\phi) = f(\phi)D_0^L$ the ϕ-dependent long-time diffusion coefficient. The factor $f(\phi)$ was estimated by extrapolating the data in Fig. 8 of Ref. [3] to $\phi = 0.60$, yielding $f \approx 1/30$. The viscoelatic moduli of the two one-component glass samples were measured using a stress controlled AR2000ex rheometer and a cone-plate geometry (see Ref. [18] for additional details). In this way we obtain samples with comparable rheological properties and, according to the generalized Stokes-Einstein relation [31], also dynamics and hence a similar location with respect to the glass transition. The comparable dynamics but different polydispersities of the one-component samples imply slightly different ϕ.

Samples with constant total volume fraction $\phi \approx 0.60$ and different compositions, namely, fractions of small particles $x_s = \phi_s/\phi$, where ϕ_s is the volume fraction of small particles, are prepared by mixing the one-component samples. Despite the relatively large uncertainty in ϕ, the important control parameter of our study, x_s, has a small uncertainty, less than 1%. This is achieved by weighting the one-component samples before mixing. The mixture was successively homogenized in a vortex mixer for a few minutes and in a roller mixer for at least 12 hours.

B. Confocal microscopy

Confocal microscopy measurements were performed using a Nikon A1R-MP confocal scanning unit mounted on a Nikon Ti-U inverted microscope, with a 60× Nikon Plan Apo oil immersion objective (NA = 1.40). Each stack consists of 100 frames of 512 × 512 pixels acquired at a rate of 30 fps, except for $x_s = 0$ and 0.01, for which each stack consists of 150 frames of 512 × 512 pixels. One stack corresponds to a volume of approximately $72 \times 72 \times 30\ \mu m^3$ ($x_s = 0.0$ and 0.01) or $72 \times 72 \times 20\ \mu m^3$ ($0.1 \leqslant x_s \leqslant 0.9$). Time series of 500 stacks were acquired for five different volumes for each sample, except for $x_s = 0.0$ for which 1000 stacks were acquired. The total measurement time of a time series is $t_{meas} \approx 30\tau_B$ ($0.1 \leqslant x_s \leqslant 0.9$), $60\tau_B$ ($x_s = 0.0$), and $44\tau_B$ ($x_s = 0.01$), respectively. Coordinates and trajectories of the large particles were extracted from the time series using standard particle tracking routines [32].

III. RESULTS AND DISCUSSION

A. Dynamics

1. *Mean squared displacement and distribution of displacements*

Based on the time series of three-dimensional confocal microscopy stacks of images, particle trajectories were determined and used to calculate mean squared displacements (MSDs) $\Delta r^2(t)$ of the large spheres in mixtures with different compositions (Fig. 1):

$$\Delta r^2(t) = \left\langle r_i^2(t,t_0) - r_i^2(t_0) \right\rangle_{i,t_0}, \tag{1}$$

where t is the delay time, t_0 a time during the trajectory of a particle i, and $\langle\ \rangle_{i,t_0}$ indicates the average over all particles i in the observation volume and all times t_0.

The one-component system of large spheres ($x_s = 0.0$) presents arrested dynamics, as indicated by the plateau of the MSD extending to long delay times, with particles localized on a length scale $L/2R_L = \sqrt{\Delta r^2(t_{min})}/2R_L \approx 0.1$, with t_{min} the minimum delay time at which the MSD was measured. (Note that in samples with a less well established plateau at t_{min}, the value of the localization length L is only indicative.) The value $L/2R_L \approx 0.1$ is characteristic of a colloidal hard-sphere glass, in which particles are caged by nearest neighbors. Consistent with this observation, the distributions of particle displacements in x direction, $P(\Delta x)$, calculated for different

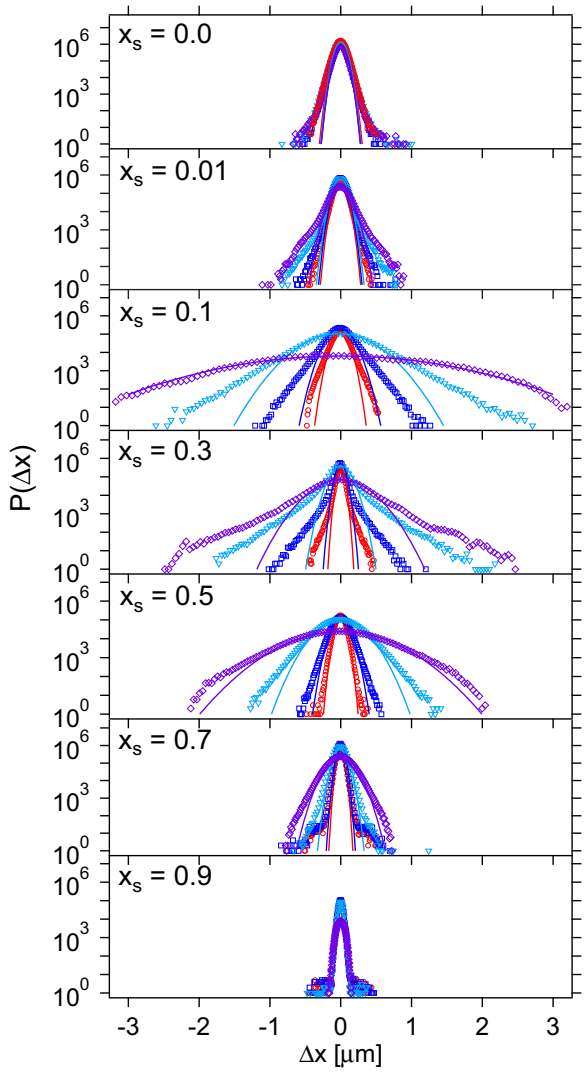

FIG. 2. (Color online) Distributions of displacements of the large spheres in x direction, $P(\Delta x)$, over delay times $\Delta t/\tau_B = 0.06$ (○), 0.3 (□), 3.0 (▽), 18.0 (♢) for samples with $\phi \approx 0.60$, $\delta = 0.09$, and different compositions x_s, as indicated. Lines represent Gaussian fits.

delay times t (Fig. 2) show hardly any evolution of the dynamics and the presence of small non-Gaussian tails, characteristic of glassy systems [5,33]. The distributions in y and z directions show similar results. For $x_s = 0.01$, the dynamics are still arrested, again indicating a glass state, with an even smaller localization length, $L/2R_L \approx 0.08$. A smaller localization length indicates a tightening of the cage. Since the volume fraction of large spheres is slightly smaller than for $x_s = 0.0$, the tightening of the cage is expected to result from the intercalation of small spheres in between large spheres and/or the exclusion of small spheres from depletion zones between large spheres, thus inducing an effective attraction (bonds) between the large spheres (see below). At long times the dynamics appear to be slightly faster than for $x_s = 0.0$. Furthermore, the distribution of displacements $P(\Delta x)$ shows comparable Gaussian contributions as the sample with $x_s = 0.0$, but more pronounced non-Gaussian tails, which indicate that the dynamics is significantly more heterogeneous (Fig. 2).

The dynamics of the mixture with $x_s = 0.1$ are not arrested (Fig. 1). Diffusive behavior is encountered at long times, while a localization plateau might exist at very short times. Due to the absence of a clear plateau, only an upper bound can be estimated for the localization length, $L/2R_L \lesssim 0.1$, which, if it exists, is smaller than that of the one-component glass. The displacement distributions $P(\Delta x)$ indicate fast dynamics, but, at short and intermediate times, also the presence of pronounced non-Gaussian tails, which again indicate significant dynamic heterogeneities. At longer times, when particles begin to diffuse, the non-Gaussian tails disappear (Fig. 2).

Increasing the amount of small spheres to $x_s = 0.3$ induces a reentrant behavior. The dynamics considerably slow down and show a subdiffusive behavior (Fig. 1). The subdiffusive dynamics suggest the presence of a broad distribution of particle mobilities, and possibly dynamical heterogeneities. This is confirmed by $P(\Delta x)$, which shows a relatively narrow, Gaussian central peak, and very long, almost exponential tails reflecting large displacements of some particles (Fig. 2). The concave shape of the tails at long times is qualitatively different from all other samples. Moreover, the localization length, $L/2R_L \lesssim 0.055$, becomes significantly smaller than that of samples with $x_s = 0.0$ and 0.01. The small localization length indicates a pronounced tightening of the cage, which again might be associated with particle-particle bonding or intercalation of small particles in between large particles (see below).

For $x_s = 0.5$ the dynamics become faster and, while still slightly subdiffusive, approach diffusion at long times. The localization length, $L/2R_L \approx 0.07$, is also significantly larger compared to $x_s = 0.3$. The non-Gaussian tails in $P(\Delta x)$ are considerably less pronounced and have a different shape than for $x_s = 0.3$, suggesting less heterogeneous dynamics. Further increasing the amount of small spheres to $x_s = 0.7$ the dynamics slow down but are still almost diffusive. Furthermore, the non-Gaussian contributions in $P(\Delta x)$ are much smaller than for $x_s = 0.5$, indicating a decreasing dynamical heterogeneity. At the same time, the localization length, $L/2R_L \approx 0.056$ is smaller than for $x_s = 0.5$ and rather comparable to $x_s = 0.3$. For $x_s = 0.9$ the dynamics are again arrested and the localization length becomes even smaller, $L/2R_L \approx 0.05$, about a factor 2 smaller than in the one-component glass of large particles (Fig. 1). Also $P(\Delta x)$ is very narrow with hardly any evolution of the dynamics and very small non-Gaussian tails (Fig. 2). In summary, both the localization length L and the degree of diffusivity of the long-time dynamics indicate a bimodal shape as a function of x_s, which reflects the transition between different arrested states, characterized by melting and the formation of fluid states.

2. *Spatial distribution of mobile particles*

Beyond the average dynamics of the large particles, quantified by $\Delta r^2(t)$ and $P(\Delta x)$, we investigated the spatial distribution of single particle mobilities, in particular whether they show spatial heterogeneities [34], and whether they are related to the spatial distribution of the small spheres. The particles which, in a given sample, perform the 20% largest displacements over a time interval of about $\tau_B/4$ are identified and highlighted in Fig. 3 [35]. Qualitatively similar results are obtained for longer time intervals; time intervals up to $5\tau_B$ are

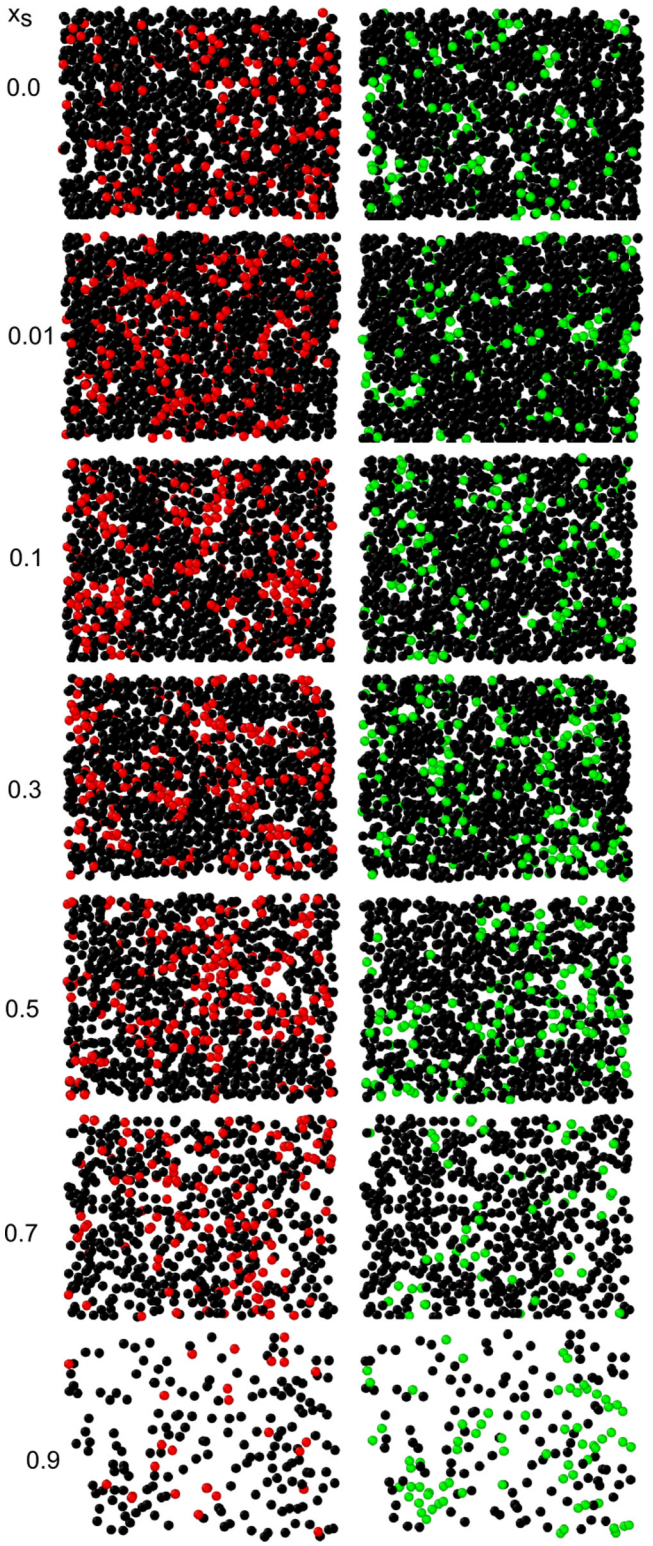

FIG. 3. (Color online) Rendering of 3 μm thick slices of a central region of 44×33 μm^2, in the bulk of samples with $\phi \approx 0.60$, $\delta = 0.09$ and different compositions x_s (as indicated) as obtained from coordinates extracted from confocal microscopy images. Left: Large particles with the 20% largest displacements over a time interval of about $\tau_B/4$ are shown in red (light gray). Right: Large particles with the 20%–30% smallest number of bonds per particle are shown in green (light gray). The small particles are not shown.

examined. In the fluid samples the dynamical heterogeneities reduce once the diffusive regime is reached.

In the one-component glass of large spheres, $x_s = 0.0$, the particles with a large mobility appear to be grouped in small clusters, which are randomly distributed in the sample. For $x_s = 0.01$, the 20% fastest particles are still distributed throughout the sample, but seem to coincide with regions with only few large spheres and a clear majority of small particles (which are not visible and therefore appear as voids in the images). This correlation becomes particularly evident in mixtures with $x_s = 0.1$, 0.3, and 0.5. This suggests that contact with the more mobile small spheres enhances the dynamics of the large spheres, as already observed in mixtures with smaller size asymmetry [36,37]. Further increasing x_s, the large particles become more dilute and hence the voids expand. Concomitantly, the most mobile particles again become more homogeneously distributed in the sample.

B. Structure

1. Pair distribution function

The particle positions calculated using the confocal micrographs allow us to determine the pair distribution function $g(r) = N(r)/4\pi\rho r^2\, dr$, with $N(r)$ the number of particles in a shell of thickness dr at distance r from a selected particle and $\rho = 3\phi/(4\pi R_L^3)\{1 - x_s(1 - 1/\delta^3)\}$ the average bulk number density of colloids (Fig. 4). For all x_s the $g(r)$ indicate an amorphous ordering, with the first peak representing the first shell of nearest neighbors and the following peaks the successive shells. The increasing dilution of the large spheres with increasing x_s is evident in the snapshots in Fig. 3 and also in the $g(r)$ for small and large x_s; the first peak decreases and shifts to larger interparticle distances, and the fluctuations at longer distances become less pronounced. However, at intermediate x_s, additional effects like bonding and structural heterogeneity, also visible in Fig. 3, lead to nonmonotonic and nontrivial variations of the heights, areas, and positions of the peaks and minima as a function of x_s (Fig. 5).

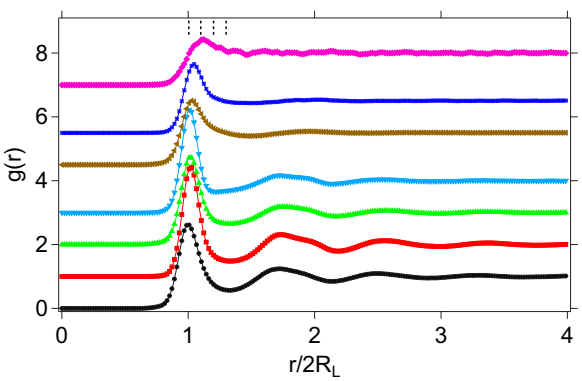

FIG. 4. (Color online) Pair distribution function $g(r)$ of large particles with radius R_L in mixtures with $\phi \approx 0.60$, $\delta = 0.09$ and different compositions $x_s = 0.0$ (●), 0.01 (■), 0.1 (▲), 0.3 (▼), 0.5 (◀), 0.7 (∗), 0.9 (♦). Data for $x_s > 0$ are shifted vertically for clarity. Dashed lines indicate particle-particle distances $r = 2R_L$, $r = 2(R_L+R_s)$, $r = 2(R_L+2R_s)$, and $r = 2(R_L+3R_s)$.

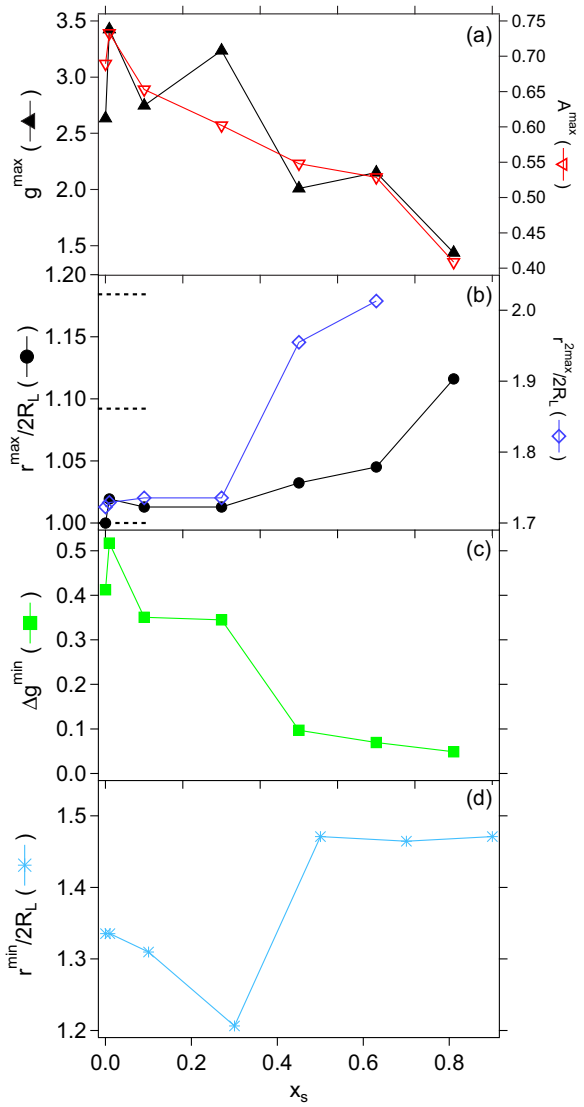

FIG. 5. (Color online) (a) Value of the pair distribution function $g(r)$, shown in Fig. 4, at the first peak, g^{max} (left y axis) and peak area A^{max}(right y axis), (b) position of the first peak $r^{max}/2R_L$ (left y axis) and second peak $r^{2max}/2R_L$ (right y axis), dashed lines indicate particle-particle distances $r = 2R_L$, $r = 2(R_L+R_s)$, $r = 2(R_L+2R_s)$, (c) depth of the first minimum $\Delta g^{min} = 1 - g(r^{min})$, and (d) position of the first minimum $r^{min}/2R_L$, as a function of x_s.

Upon addition of a tiny fraction of small spheres, i.e., from $x_s = 0.0$ to $x_s = 0.01$, the height g^{max} and area A^{max} of the first peak increase, while its position r^{max} shifts to slightly larger values [Figs. 5(a) and 5(b)]. Thus, while the large spheres are slightly diluted and hence the peak is shifted, their contacts are more pronounced, suggesting the formation of particle-particle bonds. Hence the reduction of the localization length in the MSD of this sample (Fig. 1) seems to be associated to bond formation rather than to the intercalation of small particles between the large spheres, which is supported by the fact that $r^{max} < 2(R_L+R_s)$.

With the addition of a larger fraction of small spheres, $x_s = 0.1$, the first peak remains at approximately the same position, but its height g^{max} and area A^{max} decrease, and it becomes broader [Figs. 4, 5(a), and 5(b)], indicating a smaller number of particles in the first shell of neighbors. In contrast, the first minimum shifts to smaller distances and becomes less pronounced [Figs. 4, 5(c), and 5(d)]. A less pronounced first peak could be related to the increasing dilution of the large spheres, but, together with its broadening and the shifted and flatter first minimum, might also indicate a more heterogeneous structure, possibly associated with cluster formation. An increase of the structural heterogeneity is also evidenced by the snapshots shown in Fig. 3 and will be discussed in more detail below.

For $x_s = 0.3$ the first peak increases in height but decreases in area with respect to $x_s = 0.1$ while it remains at the same position [Figs. 4, 5(a), and 5(b)]. This suggests that on average there are less particles in the first shell, which, however, tend to be in closer contact. The first minimum shifts to considerably smaller distances [Figs. 4 and 5(d)]. Its depth is comparable to that of $x_s = 0.1$ [Figs. 4 and 5(c)], but it is much more extended with the second maximum becoming less pronounced (Fig. 4). This indicates a further increase of structural heterogeneity, which is also evident in the snapshots of Fig. 3 and might reflect the dynamical heterogeneities described above (Sec. III A).

Further increasing x_s to 0.5 the height g^{max} and area A^{max} of the first peak decrease significantly and the first peak moves to larger values of r [Figs. 4, 5(a), and 5(b)]. At the same time the peak broadens and an extended shoulder is observed in between the main peak and the first minimum at $r/2R_L \approx 1.5$, which is also more pronounced [Figs. 4 and 5(c)]. The relatively weak second maximum is now located at $r/2R_L \approx 2.0$, i.e., at a distance corresponding to a second spherical shell of neighbors. The shift of the peaks and minimum to larger distances, and the decrease of the first peak height g^{max} and area A^{max}, are consistent with the progressive dilution of the large spheres, their looser structural organization and the reduction of the number of particle contacts. At the same time, the reduction of the peak and its broadening with an extended shoulder between the first peak and first minimum also indicate the presence of structural heterogeneity, also visible in Fig. 3.

If the fraction of small spheres is further increased to $x_s = 0.7$ and 0.9, the first and second peaks again shift to larger distances, and the first peak height g^{max} and area A^{max} are reduced [Figs. 4, 5(a), and 5(b)]. The first minimum, while staying at the same location, becomes increasingly more shallow [Figs. 4, 5(c), and 5(d)]. Furthermore, the shoulder in between the main peak and first minimum is less pronounced at $x_s = 0.7$ and disappears at $x_s = 0.9$ (Fig. 4). This suggests that the structural organization of the large spheres tends to that of a fluid of isolated large particles and the large particles appear as homogeneously distributed impurities in the dense structure of small spheres (Fig. 3). For $x_s = 0.9$, however, $g(r)$ is significantly different from that of a one-component dispersion of large spheres with volume fraction $\phi(1 - x_s) = 0.06$. The first peak is observed at $r \approx 2R_L+2R_s$, corresponding to a configuration in which two large particles are separated by a small particle, an "extended dimer configuration." The existence of such dimers is attributed to the depletion interactions at this large size disparity.

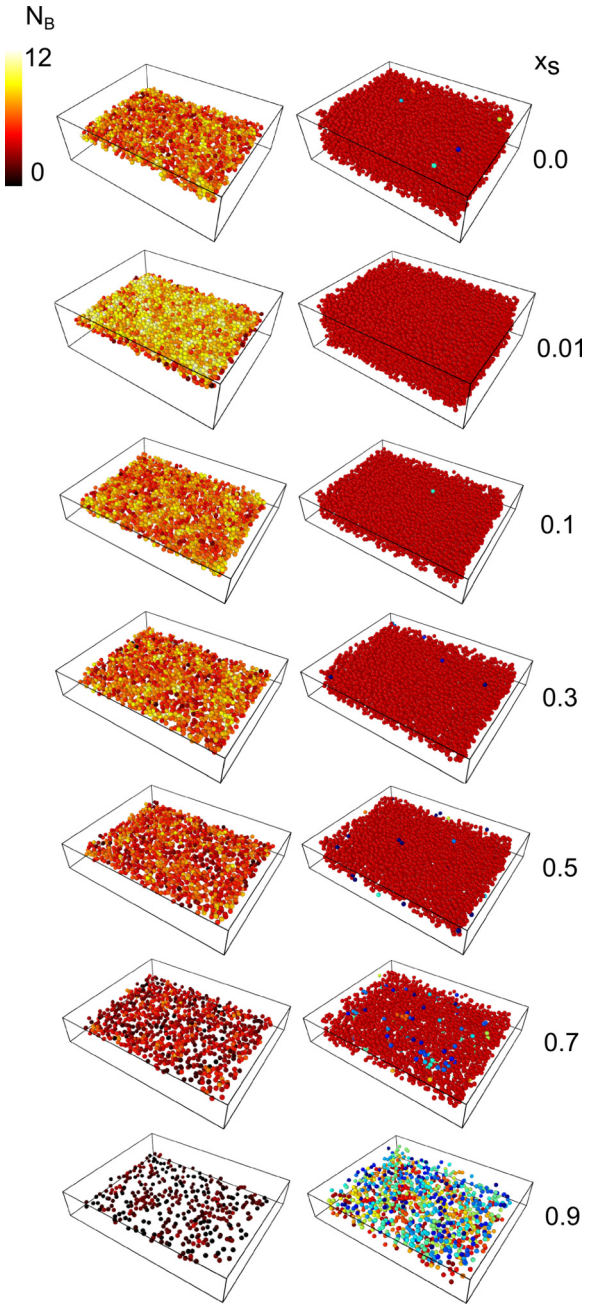

FIG. 6. (Color online) Left: Rendering of 4 μm thick slices of area $58 \times 42\,\mu\text{m}^2$ in the bulk of samples with $\phi \approx 0.60$, $\delta = 0.09$ and different compositions x_s (as indicated) as obtained from coordinates extracted from confocal microscopy images. (Left) Large particles have different color (gray-scale value) according to their number of bonds N_B (as indicated). (Right) Large particles pertaining to the same cluster are indicated with the same color (gray-scale value). The small particles are not shown.

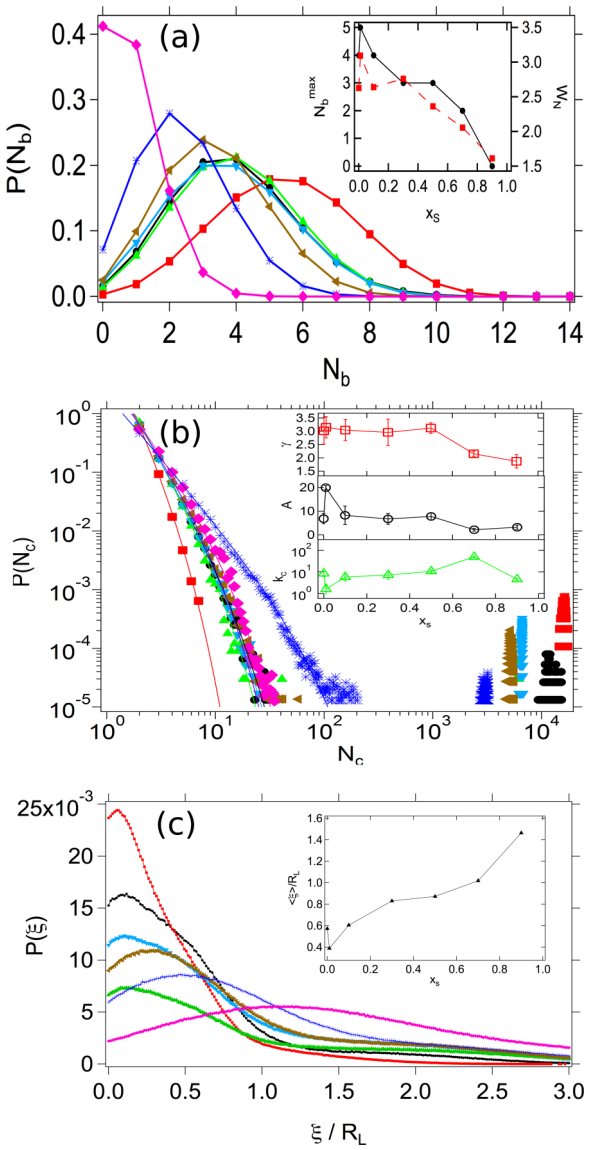

FIG. 7. (Color online) (a) Distribution of the number of bonds N_b per large particle, $P(N_b)$. Inset: Most likely number of bonds N_b^{max} (●, left axis) and width W_N of $P(N_b)$ (■, right) as a function of composition x_s. (b) Cluster size distribution $P(N_c)$, with N_c the number of particles forming the cluster. Lines are fits of a power-law dependence $f(N_c) = AN_c^{-\gamma}\exp(-N_c/k_c)$. Inset: Fit parameters A, γ, and k_c as a function of x_s (c) Remoteness distribution, $P(\xi)$, Inset: Average remoteness $\langle\xi\rangle$ as a function of x_s. The mixtures had $\phi \approx 0.60$, $\delta = 0.09$ and different compositions $x_s = 0.0$ (●), 0.01 (■), 0.1 (▲), 0.3 (▼), 0.5 (◀), 0.7 (∗), 0.9 (♦).

2. *Particle bonds and cluster sizes*

We analyzed in more detail the formation and rearrangement of network structures by determining the number of bonds per particle, N_b, as well as its distribution, $P(N_b)$. Two particles are considered bonded if their centers are closer than the first minimum of $g(r)$ of the sample with $x_s = 0.0$, i.e., if $r \leqslant 2.85R_L$. We verified that slightly different definitions of the bond length do not qualitatively affect the results. The samples are then rendered with the particles colored according to their number of bonds (Fig. 6, left) [35] and the corresponding distribution of the number of bonds $P(N_b)$ is calculated taking into account and averaging all stacks of a time series [Fig. 7(a)]. For the one-component purely repulsive hard-sphere glass also particle-particle bonds are identified due to the definition of the bond length (Fig. 6, left). The distribution of bonds per particle presents a maximum for $N_b^{max} = 4$ [Fig. 7(a)]. For $x_s = 0.01$, there is a significant

increase in N_b (Fig. 6) and, accordingly, the distribution shifts to larger values of N_b, with the maximum occurring at $N_b^{max} = 5$, and becomes broader [Fig. 7(a)]. The number of bonds decreases again for $x_s = 0.1$ (Fig. 6), and the distribution is almost identical to that of $x_s = 0.0$, suggesting that small particles start to intercalate between large particles breaking part of the bonds present for $x_s = 0.01$. Upon a dilution of the large spheres to $x_s = 0.3$, N_b remains almost unchanged (Fig. 6) with only a slight shift of the distribution $P(N_b)$ to smaller values. This can be attributed to the formation of clusters within which large particles maintain their average number of bonds due to the increased local concentration of large particles. This implies that the sample becomes heterogeneous on a mesoscopic length scale, as also suggested by the increased width of $P(N_b)$ [Fig. 7(a)]. Upon further increasing x_s, however, N_b considerably decreases (Fig. 6) and the distribution shifts to progressively smaller values of N_b and becomes narrower, suggesting a decreasing structural heterogeneity. Nevertheless, bonds are present in all samples, including $x_s = 0.9$, where a significant number of dimers is found, consistent with our other findings. The x_s dependence of N_b closely resembles that of A^{max}, as expected from the criterion chosen to define a bond. Furthermore, the width of the distributions, W_N, presents a bimodal shape as a function of x_s, similar to that of the localization length L and the maximum of $g(r)$. Bonded large particles organize into clusters of different sizes, i.e., different numbers of large particles N_c belonging to the same cluster, that eventually connect to form a network. This is illustrated in Fig. 6, which shows rendered sample volumes, with particles pertaining to the same cluster having the same color. It is evident that for $x_s \leqslant 0.7$ a percolating network of bonded particles spans the whole system. This is confirmed by the distribution of cluster sizes, $P(N_c)$ [Fig. 7(b)]. Most of the particles organize into one big cluster representing the space spanning network [the data points at the far right in Fig. 7(b)], while also a few small clusters, composed of at most 100 particles, are present in these samples. [Note that $P(N_c)$ is the probability for a cluster, not for a particle to be located in a cluster, of size N_c.] Whereas the distributions are very similar for samples with $x_s = 0.0$, 0.1, 0.3, and 0.5, the mixture with $x_s = 0.01$ shows very few small clusters, suggesting a more homogeneous structure in comparison to the samples with higher x_s. For the sample with $x_s = 0.7$ a network is still present [Figs. 6 and 7(b)], but $P(N_c)$ is significantly broader for the smaller clusters, extending to sizes beyond 50 particles per cluster. This indicates a transition from a network structure of large particles to isolated clusters of large particles immersed in a "sea" of small particles. This transition is completed for $x_s = 0.9$, where no large clusters are observed.

The function $f(N_c) = AN_c^{-\gamma} \exp(-N_c/k_c)$ fits the experimental distributions $P(N_c)$, where the fit parameters A, γ, and k_c are not completely uncorrelated and thus their values have to be treated with care. The fit function is expected to describe the cluster distribution of irreversible physical gels [38]. An exponent $\gamma < 3$ indicates the presence of a space spanning network of clusters. Initially ($x_s \leqslant 0.5$) the exponent is approximately constant, $\gamma \approx 3 \pm 0.5$, and then decreases with a minimum at $x_s = 0.7$. These values of γ are consistent with the presence of a space-spannning network. The exponential cutoff k_c quantifies the limiting cluster size. It is almost constant except a minimum for $x_s = 0.01$ and a maximum for $x_s = 0.7$. The intercept A, which is related to the fraction of particles not pertaining to any cluster, shows a slight decrease except for a peak at $x_s = 0.01$ and a minimum for $x_s = 0.7$. The trends of the fit parameters are consistent with the more homogeneous structure of sample $x_s = 0.01$ and confirm the broad distribution of cluster sizes of sample $x_s = 0.7$.

3. Remoteness

In order to investigate the degree of structural heterogeneity, we determined the distribution of particle remoteness $P(\xi)$ [39,40] [Fig. 7(c)]. Particle remoteness ξ measures the distance of a point from the surface of the closest particle. A large value of the remoteness ξ is therefore an indication of large voids or open arrangements and a broad distribution of ξ of heterogeneous structures. Although our samples are densely packed with $\phi = 0.60$, we are interested in the arrangement of the large spheres only and hence consider as "void" any volume which is not occupied by large spheres. A large fraction of the voids is thus occupied by small (invisible) particles.

The one-component glass of large spheres shows a $P(\xi)$ which is peaked at a small value, $\xi \approx 0.2R_L$ and shows only a very small probability for $\xi > R_L$. This reflects the small interstitial voids between densely packed large spheres. For $x_s = 0.01$, the $P(\xi)$ is shifted to smaller ξ and the probability of large voids is further suppressed. This is also indicated by the smaller average remoteness $\langle\xi\rangle$ [Fig. 7(c), inset]. In contrast, for $x_s = 0.1$, while the main peak remains at about the same position, the distribution considerably broadens and $\xi > R_L$ becomes more probable, with a second very weak maximum at $\xi \approx 2.25R_L$ and $\langle\xi\rangle$ is increased. Thus larger unoccupied regions exist. The probability of larger ξ, including the weak maximum and $\langle\xi\rangle$, increase further for $x_s = 0.3$ while the main peak remains at $\xi \approx 0.2R_L$. This suggests the presence of a backbone of bonded particles in close contact, i.e., a network of large particles. For $x_s = 0.5$ and 0.7 the probability of large $\xi/R_L > 2$ remains almost unchanged, but the main peak shifts to larger ξ and $\langle\xi\rangle$ slightly increases while the distribution broadens. For $x_s = 0.9$ the whole distribution is significantly shifted to large values of ξ. This is an indication that the gel network starts to melt due to the increasing dilution of large spheres (increase of $\langle\xi\rangle$) and for $x_s = 0.9$ disappears, and isolated particles or "extended dimer configurations" are prevailing. The presence of a few, homogeneously distributed isolated particles or extended dimers is consistent with a more homogeneous distribution of remoteness.

C. Comparison of dynamics and structure: Glass, gel, and fluid states

1. Different arrested states

The information on the dynamics and structure is now combined to provide a comprehensive characterization of the different states as a function of the sample composition x_s.

The dynamics indicate that the one-component system of large spheres, $x_s = 0.0$, and the mixtures with a majority of one species, i.e., $x_s = 0.01$ and 0.9, as well as an intermediate composition, $x_s = 0.3$, present very slow, arrested dynamics, characteristic of glasses and gels. These samples show, however, significantly different degrees of arrest, subdiffusion and localization lengths of the large spheres. In the following we discuss these differences, and later compare the dynamically arrested states with the fluid states which occur at intermediate compositions $x_s = 0.1$ as well as $x_s = 0.5$ and 0.7.

Considering the arrested states, the localization length of the large spheres decreases continuously from $x_s = 0.0$ to 0.01, 0.3, and 0.9. In the fluid states that characterize the transitions between two arrested states, instead the localization lengths are larger. Dynamical arrest is particularly pronounced for $x_s = 0.0$ and 0.9, and less so for $x_s = 0.3$. The extended plateau in the MSD with a small localization length of sample $x_s = 0.01$ implies a tight cage and is attributed to the formation of interparticle bonds, which are characteristic for an attractive glass state. This is supported by the structural analysis; the arrangement of the large particles is amorphous although in a space spanning network with an increased average number of bonds per particle. Nevertheless, on a mesoscopic scale the large particles are homogeneously distributed with the distribution of remoteness indicating the absence of large voids unoccupied by large particles (but by small particles). Again, this is typical for an attractive glass rather than a gel. As proposed recently, caging is possibly still the origin of dynamical arrest in attractive glasses [41].

For $x_s = 0.3$ the localization length is even smaller, but the plateau and subdiffusion are less pronounced. The structure of this sample indicates that the tight localization in the dynamics is caused by a high probability for particle contacts due to depletion attraction induced by the small particles. Furthermore, the presence of significant structural heterogeneity seems responsible for the broad distribution of relaxation times leading to the subdiffusive MSD. These observations suggest a gellike state of this mixture, which is supported by the presence of a large cluster.

The mixture with $x_s = 0.9$ exhibits the smallest localization length with an extended plateau and the most pronounced dynamical arrest. There is no network in this sample, but many small clusters and a few slightly larger clusters. Furthermore, due to the large dilution, large particles are not caged by other large particles and the pair correlation function shows fluidlike particle organization. The dynamical arrest of the large particles therefore must be caused by the small particles. This suggests an asymmetric glass state, in which individual large particles or small clusters of a few large particles are caged by small particles. Due to the ability of small particles to tightly pack around large particles, these cages are smaller than cages formed by large spheres, even by attractive large spheres. Therefore, we observe four different arrested states: a repulsive glass ($x_s = 0.0$), an attractive glass ($x_s = 0.01$), a gel ($x_s = 0.3$), and an asymmetric glass ($x_s = 0.9$).

The transitions between these arrested states (except between the repulsive and attractive glasses) involve the melting of the glasses and the formation of fluids. We observe diffusive dynamics for samples with $x_s = 0.1$, separating the attractive glass and gel state, as well as $x_s = 0.5$ and 0.7, separating the gel and the asymmetric glass states. Despite the diffusive dynamics, these fluids are characterized by particle-particle bonds and dynamic networks. It is conceivable that, for $x_s = 0.1$, the volume fraction of large spheres is too small for a glass state, as it exists for $x_s = 0.01$, and the volume fraction of small spheres too small for depletion attraction to induce gelation, like for $x_s = 0.3$. For $x_s = 0.5$ and 0.7 melting can be associated with the dilution of the gel structure and thus a breakdown of the system-spanning network on one hand (from $x_s = 0.3$ to 0.5) and dilution of the glass matrix of small spheres on the other hand (from $x_s = 0.9$ to 0.7).

The comparison between arrested and fluid states indicates that the presence of a space-spanning network, defined on the basis of a structural criterion (particle distances) is not sufficient to distinguish between the two states. We thus combine structural and dynamical information. For each composition x_s, we identify the particles that, over the whole observation time $t_{meas} \approx 45\tau_B$, perform displacements which are smaller than the typical cage size of the one-component glass ($x_s = 0.0$), quantified by its localization length L (Fig. 1). We call these particles "arrested." The fraction of arrested particles as a function of x_s (Fig. 8) shows that the glass states ($x_s = 0.0$, 0.01 and 0.9) are characterized by the largest fractions of arrested particles, while the gel state ($x_s = 0.3$) presents a lower fraction, which is still larger than that of the neighbor fluid states. Then clusters of arrested particles are determined by applying the same criterion used previously to define bonded particles and are shown in Fig. 9. In the repulsive and attractive glasses ($x_s = 0.0$ and 0.01, respectively), the arrested particles form a dense space-spanning network. In contrast, for $x_s = 0.1$ there is only a small fraction of arrested particles, which in addition do not form a space-spanning network. For $x_s = 0.3$, instead, a dense space-spanning network of arrested particles is again observed. Subsequently, for $x_s = 0.5$, the arrested particles are organized in smaller clusters which are not space spanning. Again, a space-spanning but open network is observed for $x_s = 0.7$. Finally, for $x_s = 0.9$ there are only isolated arrested particles or individual small clusters of arrested particles. This suggests that the glass ($x_s = 0.0$, 0.01) and gel ($x_s = 0.3$) states are characterized by the presence of a dense space-spanning network of arrested large particles, while

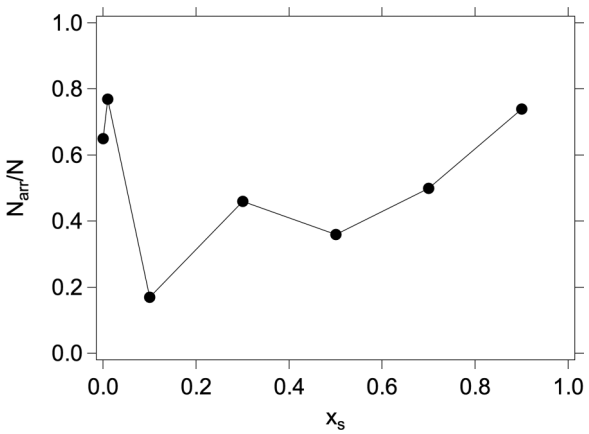

FIG. 8. Fraction of arrested particles N_{arr}/N as a function of composition x_s.

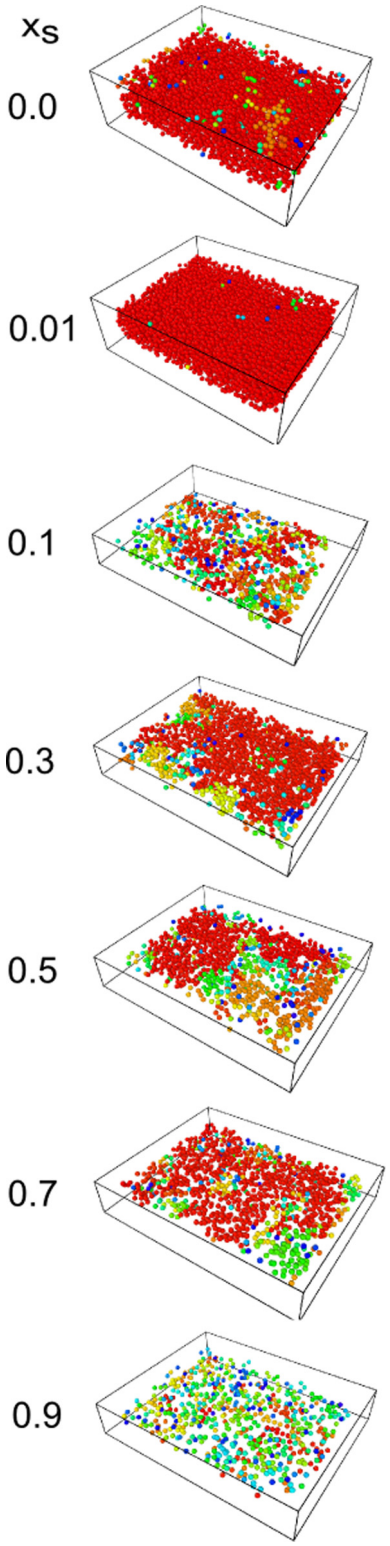

FIG. 9. (Color online) Rendering of the arrested large particles in samples with $\phi \approx 0.60$, $\delta = 0.09$, and different compositions x_s (as indicated) as obtained from trajectories extracted from confocal microscopy images. Only arrested large particles are shown with particles pertaining to the same cluster indicated with the same color (gray-scale value). Particles within two diameters of the surface of the observation volumes are not shown.

this network is not present in the fluid states ($x_s = 0.1, 0.5$) and in the asymmetric glass ($x_s = 0.9$). The sample with $x_s = 0.7$ shows an intermediate behavior.

Furthermore, we observed that in samples with a heterogeneous network structure, $0.1 \leqslant x_s \leqslant 0.7$, the fastest large particles are located in regions sparse of large particles (Fig. 3, left), and thus one might expect them to have also a smaller number of bonds with other large particles than an average particle. This, however, is true only for very few cases (Fig. 3, right). Therefore, despite their lower local volume fraction they typically maintain their number of bonds. This suggests that the fast particles form anisotropic clusters with other large particles, which allows them to keep their average coordination with other large particles while increasing the number of contacts with small particles. This could increase their mobility due to the vicinity of the more mobile small particles. Moreover, the mobility of the particles also depends on the strength (or rather weakness) of the bonds, which is experimentally not accessible to us.

2. *Dependence on size disparity*

We compare these findings with results obtained in previous work for $\delta = 0.38$ and 0.2 [17–19] as well as previous experiments for $\delta = 0.1$ [13] and theory predictions [11,12]. They are summarized in a state diagram as a function of composition x_s and size ratio δ (Fig. 10). In binary mixtures with $\delta = 0.38$ only a repulsive glass state is observed, while in mixtures with $\delta = 0.2$ two glass states of the large spheres are observed, namely, for small x_s a glass in which the large spheres are caged by large spheres and for large x_s an asymmetric glass. No evidence for a gel state was found. Very small values of x_s, like $x_s = 0.01$, were not investigated for $\delta = 0.2$ and therefore the existence of an attractive glass cannot be excluded. The asymmetric glass state observed for

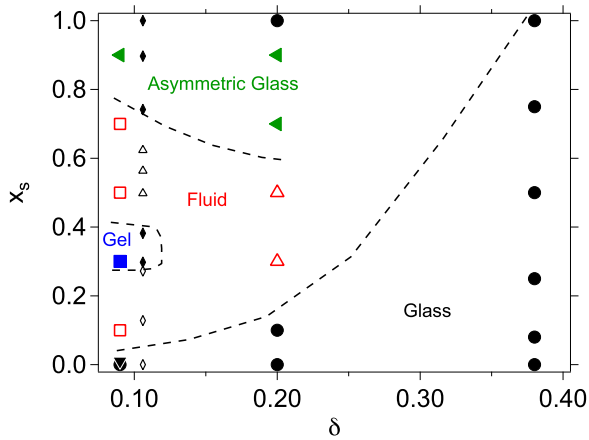

FIG. 10. (Color online) State diagram of samples with different composition x_s and size ratios; $\delta = 0.09$ (present work), $\delta = 0.106$ [13], $\delta = 0.2$ and 0.38 [17–19]. Different arrested states are identified in the present work: repulsive glass (●), attractive glass (▼), asymmetric glass (◀), and gel (■). Open symbols indicate fluid states. In [13] fluids (△), fluid-crystal coexistence (◊), and amorphous solids (⧫) were distinguished.

$\delta = 0.2$ is different from the one in this work: only individual large particles but no dimers or other small clusters were found. Since small particles can pack less effectively around dimers and small clusters than around single particles, particles forming dimers and small clusters are possibly less localized. This is consistent with the fact that for $\delta = 0.2$ the reduction of the localization length in the asymmetric glass with respect to the one-component glass, $L(x_s = 0.9)/L(x_s = 0.0) \approx 0.2 = \delta$ is considerably larger than in the case $\delta = 0.09$, namely, $L(x_s = 0.9)/L(x_s = 0.0) \approx 0.5 > \delta$.

Previous experiments on binary mixtures of silica particles with $\delta \approx 0.1$ [13] revealed an arrested state in which both components are arrested at large x_s (Fig. 10, ♦), and an arrested state in which only the large spheres are arrested at intermediate x_s (Fig. 10, ♦), while fluid-crystal coexistence was observed at small x_s (Fig. 10, ◇) and metastable fluid states at large intermediate x_s (Fig. 10, △). The arrested states of the large spheres were not further characterized in that work. Our findings suggest that the glass they observed at large x_s [13] is an asymmetric glass. Moreover, the arrested state at intermediate x_s might correspond to the gel state observed in the present work. At small x_s we find amorphous glass states or fluids, but no evidence of crystallization, which we attribute to the considerably larger polydispersity of our system, in particular of the small spheres.

Size disparities as large as $\delta = 0.1$ were not investigated by MCT or SCGLE theories [11,12]. Nevertheless, the attractive glass state observed for $x_s = 0.01$ might be related to the depletion-driven glass state predicted by MCT in this region of the phase diagram for $\delta \leqslant 0.2$ (minimum value investigated $\delta = 0.18$). Moreover, an asymmetric glass state at large x_s is predicted by MCT and SCGLE for $\delta \leqslant 0.35$. The asymmetric glass of single particles observed for $\delta = 0.2$ and $x_s = 0.9$, and predicted by theory, might be observed for $\delta = 0.09$ for values of $x_s > 0.9$. Asymmetric glass states were also reported for binary mixtures of size asymmetric star polymers [24,25], possibly indicating that in general this state is induced by a dynamical asymmetry irrespective of the details of the interaction potential.

To our knowledge, gels formed by binary mixtures have only been reported by Dinsmore and coworkers [42]. Their gels collapsed under gravity and thus represent transient states. Furthermore, gel formation in binary mixtures was observed under confinement with the addition of polymers as depletants [43]. In contrast, the gel state we observe is long lived and forms without addition of polymers but shows structural and dynamical analogies with gels formed by colloid-polymer mixtures at intermediate colloid volume fraction [44–51]; for example a large structural heterogeneity and a broad distribution of particle dynamics. The mechanism responsible for gel formation in our binary mixtures is not clear at present. Different mechanisms have been proposed for colloid-polymer mixtures, among them arrested phase separation [45,52–54], glasslike arrest [55] and rigidity percolation [56]. Moreover, equilibrium gelation in binary mixtures has been predicted as a result of the specific form of the interaction potential in these systems [16]. In order to investigate the route leading to gelation and the subsequent aging, time-resolved structural measurements are needed and will be the subject of future work.

IV. CONCLUSIONS

Different arrested states are observed for large spheres in binary mixtures with size disparity $\delta = 0.09$ and total volume fraction $\phi \approx 0.60$. While the one-component system of large spheres forms a repulsive glass, all arrested states in the mixtures are characterized by bonding, as a result of the strong depletion interaction induced by the small spheres at this size ratio. The arrested states in the mixtures significantly differ in terms of the arrest mechanism as well as structure and dynamics. If a small amount of small spheres is added to the repulsive glass of large spheres, depletion-induced attractions induce bonding and formation of an attractive glass ($x_s = 0.01$). This state is melted by further addition of small spheres ($x_s = 0.1$), possibly due to the dilution of the large spheres and a concomitant melting of the cage. Only if the amount of small spheres is increased ($x_s = 0.3$) the attraction becomes strong enough to cause dynamical arrest in the form of gelation, i.e., the formation of a network of bonded and arrested particles. This gel state shows a structural organization of the large spheres analogous to that observed in colloid-polymer mixtures. Also the gel state is melted by further dilution of the large spheres. Nevertheless, clusters of particles and a space spanning network persist ($x_s = 0.5, 0.7$) which are not arrested but fluid like. At large values of x_s an additional arrest mechanism is observed; isolated small clusters of large spheres are arrested by the highly concentrated small spheres, which possibly form a glass ($x_s = 0.9$). While asymmetric glass states were already observed for a smaller size asymmetry $\delta = 0.2$ [18,19] and for mixtures of star polymers [24,45], this asymmetric glass state is special in that depletion-induced bonding between the dilute large spheres leads to the formation of clusters, in particular "extended clusters."

Size asymmetric binary mixtures therefore represent a tunable model system to investigate transitions between different arrested states, which can be obtained by only changing the composition of the mixture. Thus the properties and behavior of different arrested states can be investigated in a consistent way using a single model system.

ACKNOWLEDGMENTS

We thank R. Castañeda-Priego, P. Chaudhuri, C. De Michele, J. Horbach, G. Petekidis, T. Sentjabrskaja, T. Voigtmann, E. Zaccarelli, and A. Zaccone for illuminating discussions. This work was funded by the Deutsche Forschungsgemeinschaft (DFG) through the research unit FOR1394, project P2. We also acknowledge funding of the confocal microscope through grant INST 208/617-1 FUGG. A.B.S. is partially funded by the UK Engineering and Physical Sciences Research Council (Grant EP/J007404/1).

[1] P. N. Pusey and W. van Megen, Nature (London) **320**, 340 (1986).

[2] P. N. Pusey, W. V. Megen, S. M. Underwood, P. Bartlett, and R. H. Ottewill, Physica A **176**, 16 (1991).

[3] W. van Megen, T. C. Mortensen, S. R. Williams, and J. Müller, Phys. Rev. E **58**, 6073 (1998).
[4] J. L. Barrat, W. Götze, and A. Latz, J. Phys.: Condens. Matter **1**, 7163 (1989).
[5] E. R. Weeks, J. C. Crocker, A. C. Levitt, A. Schofield, and D. A. Weitz, Science **287**, 627 (2000).
[6] G. Brambilla, D. El Masri, M. Pierno, L. Berthier, L. Cipelletti, G. Petekidis, and A. B. Schofield, Phys. Rev. Lett. **102**, 085703 (2009).
[7] G. L. Hunter and E. R. Weeks, Rep. Prog. Phys. **75**, 066501 (2012).
[8] S. R. Williams and W. van Megen, Phys. Rev. E **64**, 041502 (2001).
[9] G. Foffi, W. Götze, F. Sciortino, P. Tartaglia, and T. Voigtmann, Phys. Rev. Lett. **91**, 085701 (2003).
[10] W. Götze and T. Voigtmann, Phys. Rev. E **67**, 021502 (2003).
[11] T. Voigtmann, Europhys. Lett. **96**, 36006 (2011).
[12] R. Juárez-Maldonado and M. Medina-Noyola, Phys. Rev. E **77**, 051503 (2008).
[13] A. Imhof and J. K. G. Dhont, Phys. Rev. Lett. **75**, 1662 (1995).
[14] A. Moreno and J. Colmenero, J. Chem. Phys. **125**, 164507 (2006).
[15] A. J. Moreno and J. Colmenero, Phys. Rev. E **74**, 021409 (2006).
[16] P. Germain and S. Amokrane, Phys. Rev. Lett. **102**, 058301 (2009).
[17] T. Sentjabrskaja, D. Guu, M. P. Lettinga, S. U. Egelhaaf, and M. Laurati, AIP Conf. Proc. **1518**, 206 (2013).
[18] T. Sentjabrskaja, R. Babaliari, J. Hendricks, M. Laurati, G. Petekidis, and S. U. Egelhaaf, Soft Matter **9**, 4524 (2013).
[19] T. Sentjabrskaja, M. Hermes, W. C. K. Poon, C. D. Estrada, R. Castañeda-Priego, S. U. Egelhaaf, and M. Laurati, Soft Matter **10**, 6546 (2014).
[20] P. Yunker, Z. Zhang, and A. G. Yodh, Phys. Rev. Lett. **104**, 015701 (2010).
[21] S. Sanyal and A. K. Sood, Phys. Rev. E **57**, 908 (1998).
[22] T. Hamanaka and A. Onuki, Phys. Rev. E **75**, 041503 (2007).
[23] F. Ebert, P. Keim, and G. Maret, Eur. Phys. J. E **26**, 161 (2008).
[24] C. Mayer, E. Zaccarelli, E. Stiakakis, C. N. Likos, F. Sciortino, A. Munam, M. Gauthier, N. Hadjichristidis, H. Iatrou, P. Tartaglia, H. Löwen, and D. Vlassopoulos, Nat. Mater. **7**, 780 (2008).
[25] C. Mayer, F. Sciortino, C. N. Likos, P. Tartaglia, H. Löwen, and E. Zaccarelli, Macromolecules **42**, 423 (2009).
[26] C. P. Royall, W. C. K. Poon, and E. R. Weeks, Soft Matter **9**, 17 (2013).
[27] P. N. Pusey, J. Phys. France **48**, 709 (1987).
[28] A. Yethiraj and A. van Blaaderen, Nature (London) **421**, 513 (2003).
[29] W. Schaertl and H. Silescu, J. Stat. Phys. **77**, 1007 (1994).
[30] W. C. K. Poon, E. R. Weeks, and C. P. Royall, Soft Matter **8**, 21 (2012).
[31] T. G. Mason, Rheol. Acta **39**, 371 (2000).
[32] J. C. Crocker and D. G. Grier, J. Colloid Interface Sci. **179**, 298 (1996).
[33] W. K. Kegel and A. van Blaaderen, Science **287**, 290 (2000).
[34] L. Berthier, G. Biroli, J.-P. Bouchaud, L. Cipelletti, and W. van Saarloos, *Dynamical Heterogeneities in Glasses, Colloids, and Granular Media (International Series of Monographs on Physics)* (Oxford University Press, New York, 2011).
[35] A. Stukowski, Modelling Simul. Mater. Sci. Eng. **18**, 015012 (2010).
[36] J. M. Lynch, G. C. Cianci, and E. R. Weeks, Phys. Rev. E **78**, 031410 (2008).
[37] T. Narumi, S. V. Franklin, K. W. Desmond, M. Tokuyama, and E. R. Weeks, Soft Matter **7**, 1472 (2011).
[38] A. Zaccone, H. H. Winter, M. Siebenbürger, and M. Ballauff, J. Rheol. **58**, 1219 (2014).
[39] R. M. L. Evans and M. D. Haw, Europhys. Lett. **60**, 404 (2002).
[40] M. D. Haw, Soft Matter **2**, 950 (2006).
[41] E. Zaccarelli and W. C. K. Poon, Proc. Natl. Acad. Sci. USA **106**, 15203 (2009).
[42] A. D. Dinsmore, A. G. Yodh, and D. J. Pine, Phys. Rev. E **52**, 4045 (1995).
[43] R. Pandey and J. C. Conrad, Soft Matter **9**, 10617 (2013).
[44] W. C. K. Poon, J. Phys.: Condens. Matter **14**, R859 (2002).
[45] E. Zaccarelli, J. Phys.: Condens. Matter **19**, 323101 (2007).
[46] M. Laurati, G. Petekidis, N. Koumakis, F. Cardinaux, A. B. Schofield, J. M. Brader, M. Fuchs, and S. U. Egelhaaf, J. Chem. Phys. **130**, 134907 (2009).
[47] N. Koumakis and G. Petekidis, Soft Matter **7**, 2456 (2011).
[48] M. Laurati, S. U. Egelhaaf, and G. Petekidis, J. Rheol. **55**, 673 (2011).
[49] S. A. Shah, Y. L. Chen, S. Ramakrishnan, K. S. Schweizer, and C. F. Zukoski, J. Phys.: Condens. Matter **15**, 4751 (2003).
[50] P. Varadan and M. J. Solomon, Langmuir **19**, 509 (2003).
[51] C. J. Dibble, M. Kogan, and M. J. Solomon, Phys. Rev. E **74**, 041403 (2006).
[52] S. Manley, H. M. Wyss, K. Miyazaki, J. C. Conrad, V. Trappe, L. J. Kaufman, D. R. Reichman, and D. A. Weitz, Phys. Rev. Lett. **95**, 238302 (2005).
[53] P. J. Lu, E. Zaccarelli, A. B. Schofield, F. Sciortino, and D. A. Weitz, Nature (London) **453**, 499 (2008).
[54] M. E. Helgeson, Y. Gao, S. E. Moran, J. Lee, M. Godfrin, A. Tripathi, A. Bose, and P. S. Doyle, Soft Matter **10**, 3122 (2014).
[55] K. Kroy, M. E. Cates, and W. C. K. Poon, Phys. Rev. Lett. **92**, 148302 (2004).
[56] A. P. R. Eberle, N. J. Wagner, and R. Castañeda-Priego, Phys. Rev. Lett. **106**, 105704 (2011).